

Non-Orthogonal Multiple Access Performance for Millimeter Wave in Vehicular Communications

Baha Eddine Youcef Belmekki^{1 2}, Abdelkrim Hamza¹, and Benoît Escrig²

¹LISIC Laboratory, Electronic and Computer Faculty, USTHB, Algiers, Algeria,
email: {bbelmekki, ahamza}@usthb.dz

²University of Toulouse, IRIT Laboratory, School of ENSEEIHT, Institut National Polytechnique de Toulouse,
France, e-mail: {bahaeddine.belmekki, benoit.escrig}@enseeiht.fr

Abstract

In this paper, we study the performance of millimeter wave (mmWave) vehicular communications (VCs) using non-orthogonal multiple access scheme (NOMA) at road intersections, since there areas are more prone to accidents. We study the case when the intersection involves two perpendicular lanes, we then extend the study to an intersection with several lanes. The transmission occurs between a source, and two destinations. The transmission experiences interference originated from a set of vehicles that are distributed as a Poisson point process (PPP). Our analysis includes the effects of blockage from buildings and vehicles at intersections. Closed form outage probability expressions are obtained. We show that as the nodes reach the intersection, the outage probability increases. Counter-intuitively, we show that the non line of sight (NLOS) scenario has a better performance than the line of sight (LOS) scenario. Finally, we compare the performance of mmWave NOMA with OMA, and we show that NOMA offers a significant improvement over OMA mmWave vehicular networks. The analysis is verified by Monte-Carlo simulation.

Index Terms

5G, NOMA, mmWave, interference, outage probability, vehicular communications.

I. INTRODUCTION

A. Motivation

Road traffic accidents are a major issue, especially at road intersections [1]. In that regard, vehicular communications (VCs) offer several applications for road safety and traffic management. These applications can prevent accidents or alerting vehicles of accidents happening in their vicinity. Hence, these applications need high data rate and high spectral efficiency, to insure high reliability and low latency transmissions. In this context, non-orthogonal multiple access (NOMA) has been shown to increase the data rate and spectral efficiency [2]. Unlike orthogonal multiple access (OMA), NOMA allows multiple users to share the same resource with different power allocation levels. On the other hand, the needs of VCs for the fifth generation (5G) of wireless networks in terms of resources require a larger bandwidth. Since the spectral efficiency of sub-6 GHz bands has already reached the theoretical limits, millimeter wave (mmWave) frequency bands (20-100 GHz and beyond) offer a very large bandwidth [3].

B. Related Works

1) *NOMA Works*: NOMA is an efficient multiple access technique for spectrum use. It has been shown that NOMA outperforms OMA (see [4] and reference therein). However, few works investigate the effect of co-channel interference and their impact on the performance [5]–[7]. The authors in [5] and [6] analyze downlinks of NOMA networks. The authors in [8] and [7] analyze uplinks of NOMA networks. In [9], the authors analyze the performance of NOMA transmissions and propose an interference aware NOMA design that takes into account both intercell and intracell interference.

2) *mmWave Works*: In mmWave bands, few works studied communications using tools from stochastic geometry [10]–[13]. However, in [10]–[12], the effect of small-scale fading is not taken into consideration. In [13], the authors investigate the performance of mmWave relaying networks in terms of coverage probability with best relay selection.

3) *VCs at Road Intersections Works*: Several works studied the effect of the interference at intersections, considering OMA. The performance in terms of success probability are derived considering direct transmission in [14], [15]. The performance of vehicle to vehicle (V2V) communications are evaluated for multiple intersections schemes considering direct transmission in [16]. In [17], the authors derive the outage probability of a V2V communications with

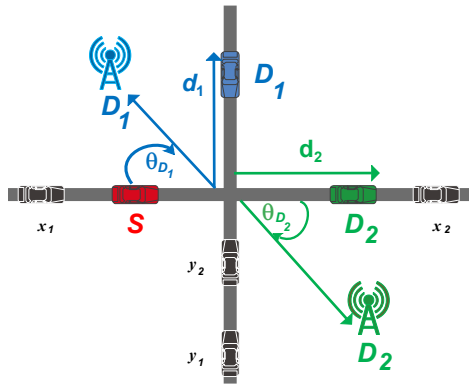


Fig. 1: NOMA system model for mmWave VCs involving a source and two destinations. The nodes can be vehicles or as part of the communication infrastructure.

power control strategy of a direct transmission. In [18], the authors investigate the impact of a line of sight and non line of sight transmissions at intersections considering Nakagami- m fading channels. The authors in [19] study the effect of mobility of vehicular communications at road junctions. In [20]–[22], the authors respectively study the impact of non-orthogonal multiple access, cooperative non-orthogonal multiple access, and maximum ratio combining with NOMA at intersections. Following this line of research, we study the performance of VCs at intersections in the presence of interference. However, at the best of the author’s knowledge, there are no prior works that consider both an intersection scenario with NOMA and considering mmWave networks. Our analysis includes the effects of blockage from the building and vehicles at intersections, and Nakagami- m fading channels between the transmitting nodes with difference values of m for LOS and NLOS are considered. Unlike other works that uses approximations, closed form expressions are obtained for Nakagami- m fading channels.

II. SYSTEM MODEL

A. Scenario Model

We consider a mm-Wave vehicular network using a NOMA transmission between a source S , and two destinations D_1 and D_2 . We consider an intersection scenario with two perpendicular roads, an horizontal road X , and a vertical road Y .

Since both V2V and V2I communications¹ are considered, any node of the triplet $\{S, D_1, D_2\}$

¹The Doppler shift and time-varying effect of V2V and V2I channels are beyond the scope of this paper.

can be on the road (e.g., vehicle), or outside the roads (e.g., infrastructure). We denote by D_i the receiving node, and by d_i the distance between the node D_i and the intersection, where $i \in \{1, 2\}$, as shown in Fig.1. The angle θ_{D_i} is the angle between the node D_i and the X road (see Fig.1).

The transmission is subject to interference that are originated from vehicles located on the roads. The set of interfering vehicles located on the X road that are in a LOS with $\{S, D_1, D_2\}$, denoted by Φ_X^{LOS} (resp. on the Y road, denoted by Φ_Y^{LOS}) are modeled as a one-dimensional homogeneous Poisson point process (1D-HPPP), that is, $\Phi_X^{\text{LOS}} \sim \text{1D-HPPP}(\lambda_X^{\text{LOS}}, x)$ (resp. $\Phi_Y^{\text{LOS}} \sim \text{1D-HPPP}(\lambda_Y^{\text{LOS}}, y)$), where x and λ_X^{LOS} (resp. y and λ_Y^{LOS}) are the position of the LOS interfering vehicles and their intensity on the X road (resp. Y road).

Similarly, the set of interfering vehicles located on the X road that are in a NLOS with $\{S, D_1, D_2\}$, denoted by Φ_X^{NLOS} (resp. on the Y road, denoted by Φ_Y^{NLOS}) are modeled as a 1D-HPPP, that is, $\Phi_X^{\text{NLOS}} \sim \text{1D-HPPP}(\lambda_X^{\text{NLOS}}, x)$ (resp. $\Phi_Y^{\text{NLOS}} \sim \text{1D-HPPP}(\lambda_Y^{\text{NLOS}}, y)$), where x and λ_X^{NLOS} (resp. y and λ_Y^{NLOS}) are the position of the NLOS interfering vehicles and their intensity on the X road (resp. Y road). The notation x and y denotes both the interfering vehicles and their locations.

B. Blockage Model

At the intersection, the mmWave signals cannot penetrate the obstacles (e.g., building, vehicles), which causes the link to be in LOS, or in NLOS. The event of a link between a node a and b is in a LOS and NLOS, are respectively defined as LOS_{ab} , and NLOS_{ab} . The LOS probability function $\mathbb{P}(\text{LOS}_{ab})$ is used, where the link between a and b has a LOS probability $\mathbb{P}(\text{LOS}_{ab}) = \exp(-\beta r_{ab})$ and NLOS probability $\mathbb{P}(\text{NLOS}_{ab}) = 1 - \mathbb{P}(\text{LOS}_{ab})$, where the constant rate β depends on the building size, shape and density [23].

C. Transmission Model

The transmission between the nodes a and b experiences a path loss, denoted $r_{ab}^{-\alpha}$, where $r_{ab} = \|a - b\|$, and α is the path loss exponent. The path exponent $\alpha \in \{\alpha_{\text{LOS}}, \alpha_{\text{NLOS}}\}$, where $\alpha = \alpha_{\text{LOS}}$, when the transmission is in LOS, whereas $\alpha = \alpha_{\text{NLOS}}$, when transmission is in NLOS.

D. Medium Access Control (MAC) Protocol

The medium access protocols used in VCs are mainly based on carrier sense multiple access (CSMA) schemes (e.g., IEEE 802.11 p) [24]. However, [25], [26] showed that the performance of

CSMA tends to the performance of ALOHA in dense networks. Hence, we assume that vehicles use slotted Aloha MAC protocol with parameter p , i.e., every node can access the medium with a probability p .

E. NOMA Model

Several works in NOMA order the receiving nodes by their channel states [27]. However, we consider that the receiving nodes are ordered according to their quality of service (QoS) priorities, since it has been show that it is more realistic assumption [28], [29]. We consider a scenario in which D_1 needs a low data rate but has to be served immediately, whereas D_2 needs a higher data rate but can be served later. This can be the case when D_1 is a vehicle that needs to receive safety data information about an accident, whereas D_2 can be a user that accesses the internet connection.

F. Directional Beamforming Model

We model the directivity similar to in [30], where the directional gain, denoted $G(\omega)$, within the half power beamwidth ($\phi/2$) is G_{max} and is G_{min} in all other directions. The gain is then expressed as

$$G(\omega) = \begin{cases} G_{max}, & \text{if } |\omega| \leq \frac{\phi}{2}; \\ G_{min}, & \text{otherwise.} \end{cases} \quad (1)$$

In this paper, we consider a perfect beam alignment between the nodes, hence $G_{eq} = G_{max}^2$. The impact of beam misalignment is beyond the scope of this paper, and can be a topic of future works.

G. Channel and Interference Model

We consider an interference limited scenario, that is, the power of noise is set to zero ($\sigma^2 = 0$). Without loss of generality, we assume that all nodes transmit with a unit power. The signal transmitted by S , denoted χ_S is a mixture of the message intended to D_1 and D_2 . This can be expressed as

$$\chi_S = \sqrt{a_1}\chi_{D_1} + \sqrt{a_2}\chi_{D_2},$$

where a_i is the power coefficients allocated to D_i , and χ_{D_i} is the message intended to D_i , where $i \in \{1, 2\}$. Since D_1 has higher power than D_2 , that is $a_1 \geq a_2$, then D_1 comes first in the

decoding order. Note that, $a_1 + a_2 = 1$.

The signal received at D_i is expressed as

$$\begin{aligned} \mathcal{Y}_{D_i} = & h_{SD_i} \sqrt{r_{SD_i}^{-\alpha}} \Upsilon \chi_S \mathbb{1}(\text{LOS}_{SD_i}) + h_{SD_i} \sqrt{r_{SD_i}^{-\alpha}} \Upsilon \chi_S \mathbb{1}(\text{NLOS}_{SD_i}) + \sum_{x \in \Phi_{X D_i}^{\text{LOS}}} h_{D_i x} \sqrt{r_{D_i x}^{-\alpha_{\text{LOS}}}} \Upsilon \chi_x \\ & + \sum_{y \in \Phi_{Y D_i}^{\text{LOS}}} h_{D_i y} \sqrt{r_{D_i y}^{-\alpha_{\text{LOS}}}} \Upsilon \chi_y + \sum_{x \in \Phi_{X D_i}^{\text{NLOS}}} h_{D_i x} \sqrt{r_{D_i x}^{-\alpha_{\text{NLOS}}}} \Upsilon \chi_x + \sum_{y \in \Phi_{Y D_i}^{\text{NLOS}}} h_{D_i y} \sqrt{r_{D_i y}^{-\alpha_{\text{NLOS}}}} \Upsilon \chi_y, \end{aligned}$$

where \mathcal{Y}_{D_i} is the signal received by D_i , and χ_S is the message transmitted by S . The messages transmitted by the interfere node x and y , are denoted respectively by χ_x and χ_y . The term $\Upsilon = G_{eq} \eta^2 / (4\pi)^2$ models the directional gain, the reference path loss at one meter, and η is the wavelength of the operating frequency.

The coefficient h_{SD_i} denotes the fading of the link $S - D_i$. The fading coefficient h_{SD_i} is distributed according to a Nakagami- m distribution with parameter m [13], that is

$$f_{h_{SD_i}}(x) = 2 \left(\frac{m}{\mu} \right)^m \frac{x^{2m-1}}{\Gamma(m)} e^{-\frac{m}{\mu} x^2}, \quad (2)$$

where the parameter $m \in \{m_{\text{LOS}}, m_{\text{NLOS}}\}$. Note that $m = m_{\text{LOS}}$ when $S - D_i$ is in a LOS, whereas $m = m_{\text{NLOS}}$, when $S - D_i$ is in a NLOS. The parameter μ is the average received power. Hence, the power fading coefficient $|h_{SD_i}|^2$ is distributed according to a gamma distribution, that is,

$$f_{|h_{SD_i}|^2}(x) = \left(\frac{m}{\mu} \right)^m \frac{x^{m-1}}{\Gamma(m)} e^{-\frac{m}{\mu} x}. \quad (3)$$

The fading coefficients $h_{D_i x}$ and $h_{D_i y}$ denote the fading of the link $D_i - x$, and $D_i - y$. The fading coefficients are modeled as Rayleigh fading [31]. Thus, the power fading coefficients $|h_{D_i x}|^2$ and $|h_{D_i y}|^2$, are distributed according to an exponential distribution with unit mean.

The aggregate interference from the X road at D_i , denoted $I_{X D_i}$, is expressed as

$$\begin{aligned} I_{X D_i} &= I_{X D_i}^{\text{LOS}} + I_{X D_i}^{\text{NLOS}} \\ &= \sum_{x \in \Phi_{X D_i}^{\text{LOS}}} |h_{D_i x}|^2 r_{D_i x}^{-\alpha_{\text{LOS}}} \Upsilon + \sum_{y \in \Phi_{X D_i}^{\text{NLOS}}} |h_{D_i x}|^2 r_{D_i x}^{-\alpha_{\text{NLOS}}} \Upsilon, \end{aligned} \quad (4)$$

where $I_{X D_i}^{\text{LOS}}$ denotes the aggregate interference from the X road that are in a LOS with D_i , and $I_{X D_i}^{\text{NLOS}}$ denotes the aggregate interference from the X road that are in a NLOS with D_i . Similarly, $\Phi_{X D_i}^{\text{LOS}}$ and $\Phi_{X D_i}^{\text{NLOS}}$, denote respectively, the set of the interferers from the X road at D_i in a LOS,

and in NLOS. In the same way, the aggregate interference from the Y road at D_i , denoted $I_{Y_{D_i}}$, is expressed as

$$\begin{aligned} I_{Y_{D_i}} &= I_{Y_{D_i}}^{\text{LOS}} + I_{Y_{D_i}}^{\text{NLOS}} \\ &= \sum_{y \in \Phi_{Y_{D_i}}^{\text{LOS}}} |h_{D_i,y}|^2 r_{D_i,y}^{-\alpha_{\text{LOS}}} \Upsilon + \sum_{y \in \Phi_{Y_{D_i}}^{\text{NLOS}}} |h_{D_i,y}|^2 r_{D_i,y}^{-\alpha_{\text{NLOS}}} \Upsilon, \end{aligned} \quad (5)$$

where $I_{Y_{D_i}}^{\text{LOS}}$ denotes the aggregate interference from the X road that are in a LOS with D_i , and $I_{Y_{D_i}}^{\text{NLOS}}$ denotes the aggregate interference from the Y road that are in a NLOS with D_i . Similarly, $\Phi_{Y_{D_i}}^{\text{LOS}}$ and $\Phi_{Y_{D_i}}^{\text{NLOS}}$, denote respectively, the set of the interferers from the Y road at D_i in a LOS, and in NLOS.

III. NOMA OUTAGE EXPRESSIONS

A. Signal-to-Interference Ratio (SIR) Expressions

The outage probability is defined as the probability that the SIR at the receiver is below a given threshold. According to successive interference cancellation (SIC) [32], D_1 message is decoded first at the receiver since it has the higher power allocation, and D_2 message is considered as interference. The SIR at D_1 to decode its desired message, denoted $\text{SIR}_{D_1}^{(\alpha)}$, is given by

$$\text{SIR}_{D_1}^{(\alpha)} = \frac{|h_{SD_1}|^2 r_{SD_1}^{-\alpha} \Upsilon a_1}{|h_{SD_1}|^2 r_{SD_1}^{-\alpha} \Upsilon a_2 + I_{X_{D_1}} + I_{Y_{D_1}}}. \quad (6)$$

In order for D_2 to decode its desired message, it has to decode D_1 message. The SIR at D_2 to decode D_1 message, denoted $\text{SIR}_{D_2-1}^{(\alpha)}$, is expressed as

$$\text{SIR}_{D_2-1}^{(\alpha)} = \frac{|h_{SD_2}|^2 r_{SD_2}^{-\alpha} \Upsilon a_1}{|h_{SD_2}|^2 r_{SD_2}^{-\alpha} \Upsilon a_2 + I_{X_{D_2}} + I_{Y_{D_2}}}. \quad (7)$$

The SIR at D_2 to decode its desired message, denoted $\text{SIR}_{D_2-2}^{(\alpha)}$, is expressed as

$$\text{SIR}_{D_2-2}^{(\alpha)} = \frac{|h_{SD_2}|^2 r_{SD_2}^{-\alpha} \Upsilon a_2}{I_{X_{D_2}} + I_{Y_{D_2}}}. \quad (8)$$

B. Outage Event Expressions

The outage event that D_1 does not decode its desired message, denoted O_{D_1} , is defined as

$$\mathcal{O}_{D_1} \triangleq \bigcup_{Z \in \{\text{LOS}, \text{NLOS}\}} \left\{ Z_{SD_1} \cap (\text{SIR}_{D_1}^{(\alpha_Z)} < \Theta_1) \right\}, \quad (9)$$

where $\Theta_1 = 2^{2\mathcal{R}_1} - 1$, and \mathcal{R}_1 is the target data rate of D_1 .

Also, the outage event that D_2 does not decode its desired message, denoted O_{D_2} , is defined as

$$\mathcal{O}_{D_2} \triangleq \bigcup_{Z \in \{\text{LOS}, \text{NLOS}\}} \bigcup_{i=1}^2 \left\{ Z_{SD_2} \cap (\text{SIR}_{D_2-i}^{(\alpha_Z)} < \Theta_i) \right\}, \quad (10)$$

where $\Theta_2 = 2^{2\mathcal{R}_2} - 1$ ($i = 2$), and \mathcal{R}_2 is the target data rate of D_2 .

C. Outage Probability Expressions

The outage probability related to \mathcal{O}_{D_1} , denoted $\mathbb{P}(\mathcal{O}_{D_1})$, is given when $\Theta_1 < \frac{a_1}{a_2}$, by

$$\mathbb{P}(\mathcal{O}_{D_1}) = 1 - \sum_{Z \in \{\text{LOS}, \text{NLOS}\}} \mathbb{P}(Z_{SD_1})$$

$$\prod_{K \in \{\text{LOS}, \text{NLOS}\}} \sum_{k=0}^{m_Z-1} \frac{1}{k!} \left(-\frac{m_Z \Psi_1}{\mu r_{SD_1}^{-\alpha_Z} \Upsilon} \right)^k \sum_{n=0}^k \binom{k}{n} \frac{d^{k-n} \mathcal{L}_{I_{X_{D_1}}^K} \left(\frac{m_Z \Psi_1}{\mu r_{SD_1}^{-\alpha_Z} \Upsilon} \right) d^n \mathcal{L}_{I_{Y_{D_1}}^K} \left(\frac{m_Z \Psi_1}{\mu r_{SD_1}^{-\alpha_Z} \Upsilon} \right)}{d^{k-n} \left(\frac{m_Z \Psi_1}{\mu r_{SD_1}^{-\alpha_Z} \Upsilon} \right) d^n \left(\frac{m_Z \Psi_1}{\mu r_{SD_1}^{-\alpha_Z} \Upsilon} \right)}, \quad (11)$$

where $\Psi_1 = \Theta_1 / (a_1 - \Theta_1 a_2)$.

The outage probability related to \mathcal{O}_{D_2} , denoted by $\mathbb{P}(\mathcal{O}_{D_2})$ is given, when $\Theta_1 < \frac{a_1}{a_2}$, by

$$\mathbb{P}(\mathcal{O}_{D_2}) = 1 - \sum_{Z \in \{\text{LOS}, \text{NLOS}\}} \mathbb{P}(Z_{SD_2})$$

$$\prod_{K \in \{\text{LOS}, \text{NLOS}\}} \sum_{k=0}^{m_Z-1} \frac{1}{k!} \left(-\frac{m_Z \Psi_{\max}}{\mu r_{SD_2}^{-\alpha_Z} \Upsilon} \right)^k \sum_{n=0}^k \binom{k}{n} \frac{d^{k-n} \mathcal{L}_{I_{X_{D_2}}^K} \left(\frac{m_Z \Psi_{\max}}{\mu r_{SD_2}^{-\alpha_Z} \Upsilon} \right) d^n \mathcal{L}_{I_{Y_{D_2}}^K} \left(\frac{m_Z \Psi_{\max}}{\mu r_{SD_2}^{-\alpha_Z} \Upsilon} \right)}{d^{k-n} \left(\frac{m_Z \Psi_{\max}}{\mu r_{SD_2}^{-\alpha_Z} \Upsilon} \right) d^n \left(\frac{m_Z \Psi_{\max}}{\mu r_{SD_2}^{-\alpha_Z} \Upsilon} \right)}, \quad (12)$$

where $\Psi_{\max} = \max(\Psi_1, \Psi_2)$, and $\Psi_2 = \Theta_2 / a_2$.

Proof: See Appendix A. ■

IV. LAPLACE TRANSFORM EXPRESSIONS

In this section, we present the Laplace transform expressions of the interference from the X road at D_i , denoted $\mathcal{L}_{I_{X_{D_i}}^K}$, and from the Y road at D_i , denoted $\mathcal{L}_{I_{Y_{D_i}}^K}$.

The Laplace transform of the interference originating from the X road at the received node denoted D_i , is expressed as

$$\mathcal{L}_{I_{X_{D_i}}^K}(s) = \exp\left(-p\lambda_X^K \int_{\mathbb{R}} \frac{1}{1 + \|x - D_i\|^{\alpha_K/s}} dx\right), \quad (13)$$

where

$$\|x - D_i\| = \sqrt{\left[d_i \sin(\theta_{D_i})\right]^2 + \left[x - d_i \cos(\theta_{D_i})\right]^2}. \quad (14)$$

The Laplace transform of the interference originating from the Y road at D_i is given by

$$\mathcal{L}_{I_{Y_{D_i}}^K}(s) = \exp\left(-p\lambda_Y^K \int_{\mathbb{R}} \frac{1}{1 + \|y - D_i\|^{\alpha_K/s}} dy\right), \quad (15)$$

where

$$\|y - D_i\| = \sqrt{\left[d_i \cos(\theta_{D_i})\right]^2 + \left[y - d_i \sin(\theta_{D_i})\right]^2}, \quad (16)$$

where θ_{D_i} is the angle between the node D_i and the X road. *Proof:* See Appendix B. ■

We only present the case when $\alpha_K = 2$ due to the lack of space. The Laplace transform expressions of the interference at D_i for an intersection scenario, when $\alpha_K = 2$ are given by

$$\mathcal{L}_{I_{X_{D_i}}^K}(s) = \exp\left(\frac{-p\lambda_X^K s\pi}{\sqrt{\left[d_i \sin(\theta_{D_i})\right]^2 + s}}\right), \quad (17)$$

and

$$\mathcal{L}_{I_{Y_{D_i}}^K}(s) = \exp\left(\frac{-p\lambda_Y^K s\pi}{\sqrt{\left[d_i \cos(\theta_{D_i})\right]^2 + s}}\right). \quad (18)$$

Proof: See Appendix C. ■

V. SIMULATIONS AND DISCUSSIONS

In this section, we evaluate the performance of mmWave VCs using NOMA at road intersections. In order to verify the accuracy of the theoretical results, Monte-Carlo simulations are carried out by averaging over 10,000 realizations of the PPPs and fading parameters. Monte Carlo simulations are carried out, and they match perfectly the theoretical results, which validates the correctness of our analysis. We set, without loss of generality, $\lambda_X^{\text{LOS}} = \lambda_Y^{\text{LOS}} = \lambda_X^{\text{NLOS}} = \lambda_Y^{\text{NLOS}} = \lambda$. $S = (0, 0)$, $D_1 = (100, 10)$, and $D_2 = (100, -10)$, $\beta = 9.5 \times 10^3$ [23], $\mu = 1$. We set $\alpha_{\text{LOS}} = 2$,

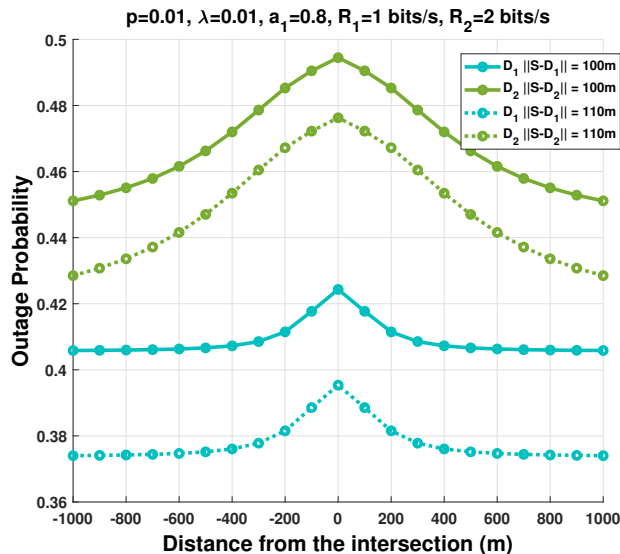


Fig. 2: Outage probability as a function of distance from the intersection.

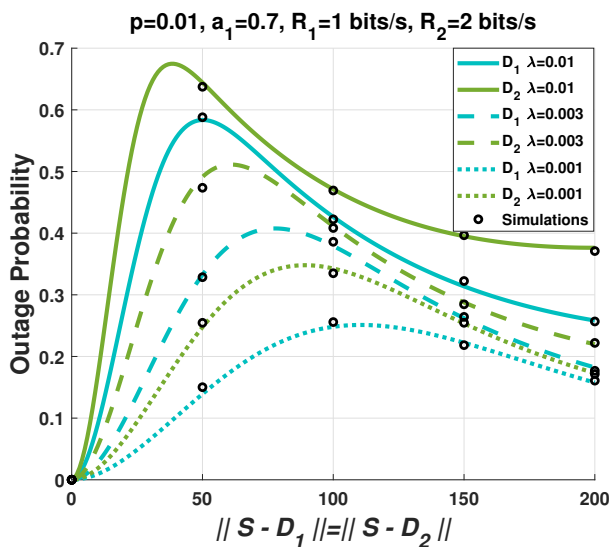


Fig. 3: Outage probability as a function of $\|S - D_1\| = \|S - D_2\|$.

$\alpha_{\text{NLOS}} = 4$, $m_{\text{LOS}} = 2$, and $m_{\text{NLOS}} = 1$. Finally, we set $G_{\text{max}} = 18$ dBi, $\eta = 30$ GHz. Unless stated otherwise, we consider mmWave VCs using NOMA in all the results.

Fig.2 shows the outage probability as a function of the distance of the triplet $\{S, D_1, D_2\}$ from the intersection. We see from Fig.2 that the outage probability increases as the vehicles drive toward the intersection. This is because when the vehicles are far from the intersection, only the interferes in the same road segment contribute to the aggregate interference. But, as the

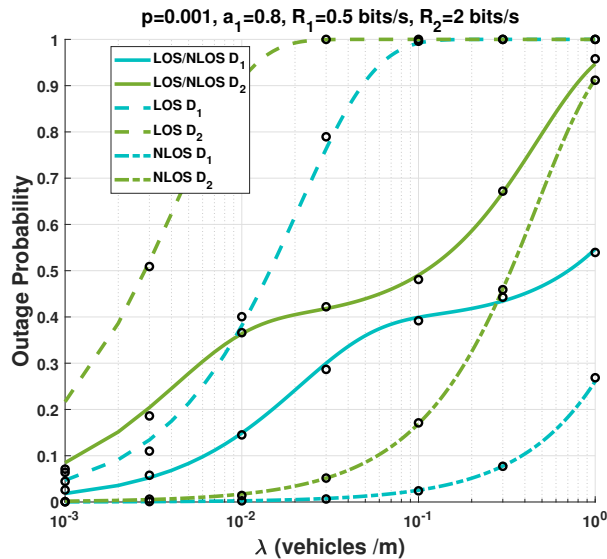


Fig. 4: Outage probability as function of λ for LOS transmission, NLOS, and LOS/NLOS (equation (11) and (12)).

vehicles approach the intersection, both road segments contribute to the aggregate interference. We can also see that the outage probability when $\|S - D_1\| = 100$ m ($\|S - D_2\| = 100$ m) is higher than the outage probability when $\|S - D_1\| = 110$ m ($\|S - D_2\| = 110$ m). This result is counter-intuitive because large distance decreases the path loss, and thus, it decreases the SIR at the receiver and increases the outage probability.

To investigate the effect of the distance between the transmitter and the receiver, Fig.3 depicts the outage probability as a function of the distance between the source and the destinations. We can see from Fig.3 that the outage probability increases, as the distance between the source and the destinations increases, until it reaches its maximum point and then it decreases. This because, as the distance between the transmitting and the receiving nodes increases, the LOS probability decreases, and the NLOS probability increases, which decreases SIR at the receiver, and hence, decreases the outage probability. We can also see that the peak of the outage probability is reached for different values of λ . In fact, we can see that for high values of λ , the peak is reached for short distances ($\|S - D_1\| = 50$ m and $\|S - D_2\| = 40$ m). However, for low values of λ , the peak is reached for high distances ($\|S - D_1\| = 110$ m and $\|S - D_2\| = 90$ m).

To show the effect of LOS and NLOS on the performance, Fig.4 plots the outage probability as function of λ for LOS transmission, NLOS transmission, and LOS/NLOS, that is equation (11) and (12). We can see that LOS scenario has the highest outage probability. This is because, when

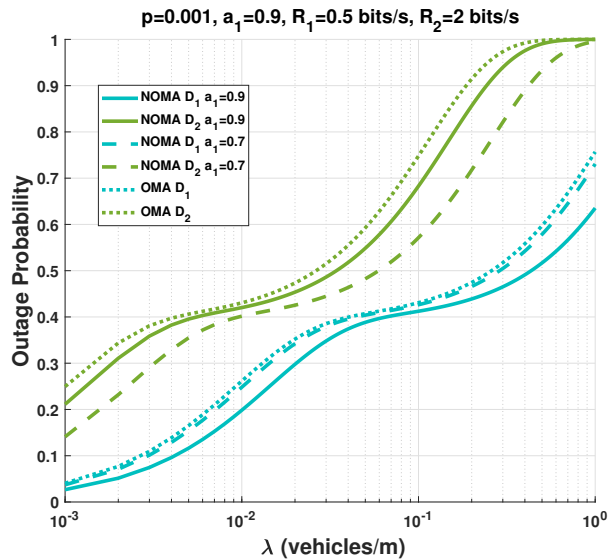


Fig. 5: Outage probability as a function of λ considering NOMA and OMA.

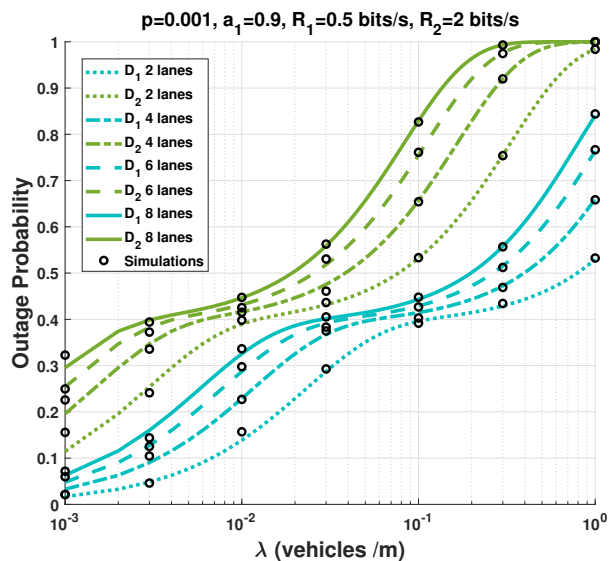


Fig. 6: Outage probability as a function of λ for several values of the number of lanes.

the interference are in direct line of sight with D_1 and D_2 , the power of aggregate interference increases, hence reducing the SIR and increasing the outage probability. On the other hand, the NLOS scenario has the smallest outage probability, since the interference are in NLOS with the transmitting nodes. The model for this paper include a blockage model that includes both LOS and NLOS. Therefore, we can see that the performance are between the LOS scenario and NLOS scenario, which are two extreme cases.

Fig.5 compares the outage probability of mmWave VCs using NOMA and OMA. We can see that NOMA outperforms OMA. We can also see that when $a_1 = 0,9$, the outage probability of D_1 decreases, and the outage probability of D_2 increases. However, when $a_1 = 0,7$, the outage probability of D_1 increases, and the outage probability of D_2 decreases. This because for low values of a_1 , there is more power allocated to D_2 , which increases its SIR and decreases its outage probability. On the other hand, high values of a_1 , means more power is allocated to D_1 , which increases its SIR and its decreases its outage probability.

Now, we investigate a more realistic intersection scenario involving several lanes. Fig.6 plots the outage probability as a function of λ for several values of the number of lanes. We can see from Fig.6 that the outage probability increases as the number of lanes increases. This because, when the number of lanes increases, the number of interfering vehicles increases as well, which increases the aggregate interference at the receiver, hence, increasing the outage probability.

VI. CONCLUSION

In this paper, we studied performance of mmWave VCs using NOMA at road intersections. We studied the case when the intersection involves of two perpendicular lanes, and then extended the study to an intersection with several lanes. Our analysis included the effects of blockage from buildings and vehicles at intersections. Closed form outage probability expressions were obtained. We showed that as the nodes reach the intersection, the outage probability increases. This makes intersections a critical areas. We also showed that that the peak of the outage probability is reached for different values of λ . We showed that for high density scenarios (high values of λ), the peak is reached for short distances, whereas for low density scenarios, the peak is reached for high distances. Counter-intuitively, we showed that NLOS scenario has a better performance than LOS scenario. Finally, we compared the performance of mmWave NOMA with OMA, and we showed that OMA offers a significant improvement over cooperative OMA.

APPENDIX A

To calculate $\mathbb{P}(\mathcal{O}_{D_1})$, we express as follows

$$\mathbb{P}(\mathcal{O}_{D_1}) = 1 - \mathbb{P}(\mathcal{O}_{D_1}^C). \quad (19)$$

The probability $\mathbb{P}(\mathcal{O}_{D_1}^C)$ is expressed as

$$\begin{aligned}
\mathbb{P}(\mathcal{O}_{D_1}^C) &= \sum_{Z \in \{\text{LOS}, \text{NLOS}\}} \mathbb{E}_{I_X, I_Y} \left[\mathbb{P} \left\{ Z_{SD_1} \cap (\text{SIR}_{D_1}^{(\alpha_Z)} \geq \Theta_1) \right\} \right] \\
&= \sum_{Z \in \{\text{LOS}, \text{NLOS}\}} \mathbb{P}(Z_{SD_1}) \mathbb{E}_{I_X, I_Y} \left[\mathbb{P} \left\{ \text{SIR}_{D_1}^{(\alpha_Z)} \geq \Theta_1 \right\} \right] \\
&= \sum_{Z \in \{\text{LOS}, \text{NLOS}\}} \mathbb{P}(Z_{SD_1}) \mathbb{E}_{I_X, I_Y} \left[\mathbb{P} \left\{ \frac{|h_{SD_1}|^2 r_{SD_1}^{-\alpha_Z} \Upsilon a_1}{|h_{SD_1}|^2 r_{SD_1}^{-\alpha_Z} \Upsilon a_2 + I_{X_{D_1}} + I_{Y_{D_1}}} \geq \Theta_1 \right\} \right] \\
&= \sum_{Z \in \{\text{LOS}, \text{NLOS}\}} \mathbb{P}(Z_{SD_1}) \mathbb{E}_{I_X, I_Y} \left[\mathbb{P} \left\{ |h_{SD_1}|^2 r_{SD_1}^{-\alpha_Z} \Upsilon (a_1 - \Theta_1 a_2) \geq \Theta_1 [I_{X_{D_1}} + I_{Y_{D_1}}] \right\} \right].
\end{aligned} \tag{20}$$

We can notice from (20) that, when $\Theta_1 \geq a_1/a_2$, $\mathbb{P}(\mathcal{O}_{D_1}^C) = 0$. Then, when $\Theta_1 < a_1/a_2$, and after setting $\Psi_1 = \Theta_1/(a_1 - \Theta_1 a_2)$, we get

$$\mathbb{P}(\mathcal{O}_{D_1}^C) = \sum_{Z \in \{\text{LOS}, \text{NLOS}\}} \mathbb{P}(Z_{SD_1}) \mathbb{E}_{I_X, I_Y} \left[\mathbb{P} \left\{ |h_{SD_1}|^2 \geq \frac{\Psi_1}{r_{SD_1}^{-\alpha_Z} \Upsilon} [I_{X_{D_1}} + I_{Y_{D_1}}] \right\} \right]. \tag{21}$$

Since $|h_{SD_1}|^2$ follows a gamma distribution, its complementary cumulative distribution function (CCDF) is given by

$$\bar{F}_{|h_{SD_1}|^2}(X) = \mathbb{P}(|h_{SD_1}|^2 > X) = \frac{\Gamma(m_Z, \frac{m_Z}{\mu} X)}{\Gamma(m_Z)}, \tag{22}$$

hence (21) becomes

$$\begin{aligned}
\mathbb{P}(\mathcal{O}_{D_1}^C) &= \sum_{Z \in \{\text{LOS}, \text{NLOS}\}} \mathbb{P}(Z_{SD_1}) \\
&\quad \mathbb{E}_{I_X, I_Y} \left[\frac{\Gamma\left(m_Z, \frac{m_Z \Psi_1}{\mu r_{SD_1}^{-\alpha_Z} \Upsilon} (I_{X_{D_1}}^{\text{LOS}} + I_{Y_{D_1}}^{\text{LOS}})\right)}{\Gamma(m_Z)} \right] \times \mathbb{E}_{I_X, I_Y} \left[\frac{\Gamma\left(m_Z, \frac{m_Z \Psi_1}{\mu r_{SD_1}^{-\alpha_Z} \Upsilon} (I_{X_{D_1}}^{\text{NLOS}} + I_{Y_{D_1}}^{\text{NLOS}})\right)}{\Gamma(m_Z)} \right].
\end{aligned}$$

Therefore, we obtain

$$\mathbb{P}(\mathcal{O}_{D_1}^C) = \sum_{Z \in \{\text{LOS}, \text{NLOS}\}} \mathbb{P}(Z_{SD_1}) \prod_{K \in \{\text{LOS}, \text{NLOS}\}} \mathbb{E}_{I_X, I_Y} \left[\frac{\Gamma\left(m_Z, \frac{m_Z \Psi_1}{\mu r_{SD_1}^{-\alpha_Z} \Upsilon} (I_{X_{D_1}}^K + I_{Y_{D_1}}^K)\right)}{\Gamma(m_Z)} \right]. \tag{23}$$

The exponential sum function when m_Z is an integer is defined as

$$e_{(m_Z)} = \sum_{k=0}^{m_Z-1} \frac{\left(\frac{m_Z}{\mu} X\right)^k}{k!} = e^X \frac{\Gamma(m_Z, \frac{m_Z}{\mu} X)}{\Gamma(m_Z)}, \tag{24}$$

then

$$\frac{\Gamma(m_Z, \frac{m_Z X}{\mu})}{\Gamma(m_Z)} = e^{-\frac{m_Z X}{\mu}} \sum_{k=0}^{m_Z-1} \frac{1}{k!} \left(\frac{m_Z X}{\mu} \right)^k. \quad (25)$$

We denote the expectation in equation (23) by $\mathcal{E}(I_X, I_Y)$, then $\mathcal{E}(I_X, I_Y)$ equals

$$\begin{aligned} \mathcal{E}(I_X, I_Y) &= \mathbb{E}_{I_X, I_Y} \left[\exp \left(- \frac{m_Z \Psi_1}{\mu r_{SD_1}^{-\alpha_Z} \Upsilon} (I_{X_{D_1}}^K + I_{Y_{D_1}}^K) \right) \sum_{k=0}^{m_Z-1} \frac{1}{k!} \left(\frac{m_Z \Psi_1}{\mu r_{SD_1}^{-\alpha_Z} \Upsilon} (I_{X_{D_1}}^K + I_{Y_{D_1}}^K) \right)^k \right] \\ &= \sum_{k=0}^{m_Z-1} \frac{1}{k!} \left(\frac{m_Z \Psi_1}{\mu r_{SD_1}^{-\alpha_Z} \Upsilon} \right)^k \mathbb{E}_{I_X, I_Y} \left[\exp \left(- \frac{m_Z \Psi_1}{\mu r_{SD_1}^{-\alpha_Z} \Upsilon} (I_{X_{D_1}}^K + I_{Y_{D_1}}^K) \right) (I_{X_{D_1}}^K + I_{Y_{D_1}}^K)^k \right]. \end{aligned} \quad (26)$$

Applying the binomial theorem in (26), we get

$$\begin{aligned} \mathcal{E}(I_X, I_Y) &= \sum_{k=0}^{m_Z-1} \frac{1}{k!} \left(\frac{m_Z \Psi_1}{\mu r_{SD_1}^{-\alpha_Z} \Upsilon} \right)^k \\ &\quad \times \mathbb{E}_{I_X, I_Y} \left[\exp \left(- \frac{m_Z \Psi_1}{\mu r_{SD_1}^{-\alpha_Z} \Upsilon} [I_{X_{D_1}}^K + I_{Y_{D_1}}^K] \right) \sum_{n=0}^k \binom{k}{n} (I_{X_{D_1}}^K)^{k-n} (I_{Y_{D_1}}^K)^n \right] \\ &= \sum_{k=0}^{m_Z-1} \frac{1}{k!} \Omega^k \mathbb{E}_{I_X, I_Y} \left[\exp \left(- \Omega [I_{X_{D_1}}^K + I_{Y_{D_1}}^K] \right) \times \sum_{n=0}^k \binom{k}{n} (I_{X_{D_1}}^K)^{k-n} (I_{Y_{D_1}}^K)^n \right], \end{aligned} \quad (27)$$

where $\Omega = \frac{m_Z \Psi_1}{\mu r_{SD_1}^{-\alpha_Z} \Upsilon}$. To calculate the expectation in (27), denoted $\mathcal{T}(I_X, I_Y)$, we proceed as follows

$$\begin{aligned} \mathcal{T}(I_X, I_Y) &= \sum_{n=0}^k \binom{k}{n} \\ &\quad \times \mathbb{E}_{I_X, I_Y} \left[e^{-\Omega I_{X_{D_1}}^K} e^{-\Omega I_{Y_{D_1}}^K} (I_{X_{D_1}}^K)^{k-n} (I_{Y_{D_1}}^K)^n \right] \\ &= \sum_{n=0}^k \binom{k}{n} \mathbb{E}_{I_X} \left[e^{-\Omega I_{X_{D_1}}^K} (I_{X_{D_1}}^K)^{k-n} \right] \\ &\quad \times \mathbb{E}_{I_{Y_{D_1}}^K} \left[e^{-\Omega I_{Y_{D_1}}^K} (I_{Y_{D_1}}^K)^n \right] \\ &\stackrel{(a)}{=} \sum_{n=0}^k \binom{k}{n} (-1)^{k-n} \frac{d^{k-n} \mathcal{L}_{I_{X_{D_1}}^K}(\Omega)}{d^{k-n} \Omega} (-1)^n \frac{d^n \mathcal{L}_{I_{Y_{D_1}}^K}(\Omega)}{d^n \Omega} \\ &= (-1)^k \sum_{n=0}^k \binom{k}{n} \frac{d^{k-n} \mathcal{L}_{I_{X_{D_1}}^K}(\Omega)}{d^{k-n} \Omega} \frac{d^n \mathcal{L}_{I_{Y_{D_1}}^K}(\Omega)}{d^n \Omega}. \end{aligned}$$

where (a) stems from the following property

$$\begin{aligned}\mathbb{E}_I \left[e^{-\Omega I} I^N \right] &= (-1)^N \frac{d^N \mathbb{E}_I \left[e^{-\Omega I} I^N \right]}{d^N \Omega} \\ &= (-1)^N \frac{d^N \mathcal{L}_I(\Omega)}{d^N \Omega}.\end{aligned}$$

Finally, the expectation becomes

$$\mathcal{T}(I_X, I_Y) = \sum_{k=0}^{m_Z-1} \frac{1}{k!} \left(-\frac{m_Z \Psi_1}{\mu r_{SD_1}^{-\alpha_Z} \Upsilon} \right)^k \sum_{n=0}^k \binom{k}{n} \frac{d^{k-n} \mathcal{L}_{I_{X_{D_1}}}^k \left(\frac{m_Z \Psi_1}{\mu r_{SD_1}^{-\alpha_Z} \Upsilon} \right) d^n \mathcal{L}_{I_{Y_{D_1}}}^k \left(\frac{m_Z \Psi_1}{\mu r_{SD_1}^{-\alpha_Z} \Upsilon} \right)}{d^{k-n} \left(\frac{m_Z \Psi_1}{\mu r_{SD_1}^{-\alpha_Z} \Upsilon} \right) d^n \left(\frac{m_Z \Psi_1}{\mu r_{SD_1}^{-\alpha_Z} \Upsilon} \right)}. \quad (28)$$

Then plugging (28) in (23) yields (11). The expression of $d^{k-n} \mathcal{L}_{I_X^k}(s)/d^{k-n}(s)$ and $d^n \mathcal{L}_{I_Y^k}(s)/d^n(s)$ are given by (37) and (38).

In the same way we express $\mathbb{P}(\mathcal{O}_{D_2}^C)$ as

$$\mathbb{P}(\mathcal{O}_{D_2}) = 1 - \mathbb{P}(\mathcal{O}_{D_2}^C). \quad (29)$$

To calculate $\mathbb{P}(\mathcal{O}_{D_2}^C)$ we proceed as follows

$$\begin{aligned}\mathbb{P}(\mathcal{O}_{D_2}^C) &= \sum_{Z \in \{\text{LOS, NLOS}\}} \mathbb{E}_{I_X, I_Y} \left[\mathbb{P} \left\{ \bigcap_{i=1}^2 \left\{ Z_{SD_2} \cap (\text{SIR}_{D_{2-i}}^{(\alpha_Z)} \geq \Theta_i) \right\} \right\} \right] \\ &= \sum_{Z \in \{\text{LOS, NLOS}\}} \mathbb{P}(Z_{SD_2}) \mathbb{E}_{I_X, I_Y} \left[\mathbb{P} \left\{ \bigcap_{i=1}^2 \text{SIR}_{D_{2-i}}^{(\alpha_Z)} \geq \Theta_i \right\} \right] \\ &= \sum_{Z \in \{\text{LOS, NLOS}\}} \mathbb{P}(Z_{SD_2}) \mathbb{E}_{I_X, I_Y} \left[\mathbb{P} \left\{ \text{SIR}_{D_{2-1}}^{(\alpha_Z)} \geq \Theta_1 \cap \text{SIR}_{D_{2-2}}^{(\alpha_Z)} \geq \Theta_2 \right\} \right]. \quad (30)\end{aligned}$$

Following the same steps as for $\mathbb{P}(\mathcal{O}_{D_1}^C)$, we get

$$\mathbb{P}(\mathcal{O}_{D_2}^C) = \mathbb{E}_{I_X, I_Y} \left[\mathbb{P} \left\{ \frac{|h_{SD_2}|^2 r_{SD_2}^{-\alpha_Z} \Upsilon a_1}{|h_{SD_2}|^2 r_{SD_2}^{-\alpha_Z} \Upsilon a_2 + I_{X_{D_2}} + I_{Y_{D_2}}} \geq \Theta_1, \frac{|h_{SD_2}|^2 r_{SD_2}^{-\alpha_Z} \Upsilon a_2}{I_{X_{D_2}} + I_{Y_{D_2}}} \geq \Theta_2 \right\} \right].$$

When $\Theta_1 > a_1/a_2$, then $\mathbb{P}(\mathcal{O}_{D_2}) = 1$, otherwise we continue the derivation. We set $\Psi_2 = \Theta_2/a_2$, then

$$\begin{aligned}\mathbb{P}(\mathcal{O}_{D_2}^C) &= \mathbb{E}_{I_X, I_Y} \left[\mathbb{P} \left\{ |h_{SD_2}|^2 \geq \frac{\Psi_1}{r_{SD_2}^{-\alpha_Z} \Upsilon} [I_{X_{D_2}} + I_{Y_{D_2}}], |h_{SD_2}|^2 \geq \frac{\Psi_2}{r_{SD_2}^{-\alpha_Z} \Upsilon} [I_{X_{D_2}} + I_{Y_{D_2}}] \right\} \right] \\ &= \mathbb{E}_{I_X, I_Y} \left[\mathbb{P} \left\{ |h_{SD_2}|^2 \geq \frac{\max(\Psi_1, \Psi_2)}{r_{SD_2}^{-\alpha_Z} \Upsilon} [I_{X_{D_2}} + I_{Y_{D_2}}] \right\} \right].\end{aligned}$$

Following the same steps as for $\mathbb{P}(\mathcal{O}_{D_1}^C)$, we obtain (12).

APPENDIX B

The Laplace transform of the interference originating from the X road at D_i is expressed as

$$\begin{aligned}
\mathcal{L}_{I_{X D_i}^K}(s) &= \mathbb{E} \left[\exp \left(-s I_{X D_i}^K \right) \right] \\
&= \mathbb{E} \left[\exp \left(- \sum_{x \in \Phi_{X D_i}^K} s |h_{D_i x}|^2 r_{D_i x}^{-\alpha_K} \right) \right] \\
&= \mathbb{E} \left[\prod_{x \in \Phi_{X D_i}^K} \exp \left(-s |h_{D_i x}|^2 r_{D_i x}^{-\alpha_K} \right) \right] \\
&\stackrel{(a)}{=} \mathbb{E} \left[\prod_{x \in \Phi_{X D_i}^K} \mathbb{E}_{|h_{D_i x}|^2, p} \left\{ \exp \left(-s |h_{D_i x}|^2 r_{D_i x}^{-\alpha_K} \right) \right\} \right] \\
&\stackrel{(b)}{=} \mathbb{E} \left[\prod_{x \in \Phi_{X D_i}^K} \frac{p}{1 + s r_{D_i x}^{-\alpha_K}} + 1 - p \right] \\
&\stackrel{(c)}{=} \exp \left(-\lambda_X^K \int_{\mathbb{R}} \left[1 - \left(\frac{p}{1 + s r_{D_i x}^{-\alpha_K}} + 1 - p \right) \right] dx \right) \\
&= \exp \left(-p \lambda_X^K \int_{\mathbb{R}} \frac{1}{1 + 1/s r_{D_i x}^{-\alpha_K}} dx \right) \tag{31} \\
&= \exp \left(-p \lambda_X^K \int_{\mathbb{R}} \frac{1}{1 + r_{D_i x}^{\alpha_K}/s} dx \right), \tag{32}
\end{aligned}$$

where (a) follows from the independence of the fading coefficients; (b) follows from performing the expectation over $|h_{D_i x}|^2$ which follows an exponential distribution with unit mean, and performing the expectation over the set of interferes; (c) follows from the probability generating functional (PGFL) of a PPP. The expression of $\mathcal{L}_{I_{Y D_i}^K}(s)$ can be acquired by following the same steps.

APPENDIX C

In order to calculate the Laplace transform of interference originated from the X road at the node D_i , we have to calculate the integral in (13). We calculate the integral in (13) for $\alpha_K = 2$. We set $d_{ix} = d_i \cos(\theta_{D_i})$, and $d_{iy} = d_i \sin(\theta_{D_i})$, then (13) becomes

$$\mathcal{L}_{I_{X D_i}^K}(s) = \exp \left(-p \lambda_X^K s \int_{\mathbb{R}} \frac{1}{s + d_{iy}^2 + (x - d_{ix})^2} dx \right), \tag{33}$$

and the integral inside the exponential in (33) equals

$$\int_{\mathbb{R}} \frac{1}{s + d_{iy}^2 + (x - d_{ix})^2} dx = \frac{\pi}{\sqrt{d_{iy}^2 + s}}. \quad (34)$$

Then, plugging (34) into (33), and substituting d_{iy} by $d_i \sin(\theta_{D_i})$ we obtain

$$\mathcal{L}_{I_{X_{D_i}}^K}(s) = \exp\left(-\frac{p\lambda_X^K s \pi}{\sqrt{d_i^2 \sin^2(\theta_{D_i}) + s}}\right). \quad (35)$$

Following the same steps above, and without details for the derivation with respect to s , we obtain

$$\mathcal{L}_{I_{Y_{D_i}}^K}(s) = \exp\left(-\frac{p\lambda_Y^K s \pi}{\sqrt{d_i^2 \cos^2(\theta_{D_i}) + s}}\right). \quad (36)$$

Then, when compute the derivative of (35) and (36), we obtain

$$\begin{aligned} \frac{d^{k-n} \mathcal{L}_{I_{X_{D_i}}^K}(s)}{d^{k-n} s} &= \left[-\frac{p\lambda_X^K \pi}{\sqrt{d_i^2 \sin^2(\theta_{D_i}) + s}} + \frac{1}{2} \frac{p\lambda_X^K \pi s}{(d_i^2 \sin^2(\theta_{D_i}) + s)^{3/2}} \right]^{k-n} \\ &\quad \times \exp\left(-\frac{p\lambda_X^K \pi s}{\sqrt{d_i^2 \sin^2(\theta_{D_i}) + s}}\right). \end{aligned} \quad (37)$$

$$\begin{aligned} \frac{d^n \mathcal{L}_{I_{Y_{D_i}}^K}(s)}{d^n s} &= \left[-\frac{p\lambda_Y^K \pi}{\sqrt{d_i^2 \cos^2(\theta_{D_i}) + s}} + \frac{1}{2} \frac{p\lambda_Y^K \pi s}{(d_i^2 \cos^2(\theta_{D_i}) + s)^{3/2}} \right]^n \\ &\quad \times \exp\left(-\frac{p\lambda_Y^K \pi s}{\sqrt{d_i^2 \cos^2(\theta_{D_i}) + s}}\right). \end{aligned} \quad (38)$$

REFERENCES

- [1] U.S. Dept. of Transportation, National Highway Traffic Safety Administration, "Traffic safety facts 2015," Jan. 2017.
- [2] Z. Ding, Y. Liu, J. Choi, Q. Sun, M. Elkashlan, I. Chih-Lin, and H. V. Poor, "Application of non-orthogonal multiple access in lte and 5g networks," *IEEE Communications Magazine*, vol. 55, no. 2, pp. 185–191, 2017.
- [3] W. Roh, J.-Y. Seol, J. Park, B. Lee, J. Lee, Y. Kim, J. Cho, K. Cheun, and F. Aryanfar, "Millimeter-wave beamforming as an enabling technology for 5g cellular communications: Theoretical feasibility and prototype results," *IEEE communications magazine*, vol. 52, no. 2, pp. 106–113, 2014.

- [4] Z. Mobini, M. Mohammadi, H. A. Suraweera, and Z. Ding, "Full-duplex multi-antenna relay assisted cooperative non-orthogonal multiple access," *arXiv preprint arXiv:1708.03919*, 2017.
- [5] K. S. Ali, H. ElSawy, A. Chaaban, M. Haenggi, and M.-S. Alouini, "Analyzing non-orthogonal multiple access (noma) in downlink poisson cellular networks," in *Proc. of IEEE International Conference on Communications (ICC18)*, 2018.
- [6] Z. Zhang, H. Sun, R. Q. Hu, and Y. Qian, "Stochastic geometry based performance study on 5g non-orthogonal multiple access scheme," in *Global Communications Conference (GLOBECOM), 2016 IEEE*, pp. 1–6, IEEE, 2016.
- [7] H. Tabassum, E. Hossain, and J. Hossain, "Modeling and analysis of uplink non-orthogonal multiple access in large-scale cellular networks using poisson cluster processes," *IEEE Transactions on Communications*, vol. 65, no. 8, pp. 3555–3570, 2017.
- [8] Z. Zhang and R. Q. Hu, "Uplink non-orthogonal multiple access with fractional power control," in *Wireless Communications and Networking Conference (WCNC), 2017 IEEE*, pp. 1–6, IEEE, 2017.
- [9] K. S. Ali, H. ElSawy, A. Chaaban, and M.-S. Alouini, "Non-orthogonal multiple access for large-scale 5g networks: Interference aware design," *IEEE Access*, vol. 5, pp. 21204–21216, 2017.
- [10] S. Biswas, S. Vuppala, J. Xue, and T. Ratnarajah, "On the performance of relay aided millimeter wave networks," *IEEE Journal of Selected Topics in Signal Processing*, vol. 10, no. 3, pp. 576–588, 2016.
- [11] S. Wu, R. Atat, N. Mastrorade, and L. Liu, "Coverage analysis of d2d relay-assisted millimeter-wave cellular networks," in *2017 IEEE Wireless Communications and Networking Conference (WCNC)*, pp. 1–6, IEEE, 2017.
- [12] K. Belbase, C. Tellambura, and H. Jiang, "Two-way relay selection for millimeter wave networks," *IEEE Communications Letters*, vol. 22, no. 1, pp. 201–204, 2018.
- [13] K. Belbase, Z. Zhang, H. Jiang, and C. Tellambura, "Coverage analysis of millimeter wave decode-and-forward networks with best relay selection," *IEEE Access*, vol. 6, pp. 22670–22683, 2018.
- [14] E. Steinmetz, M. Wildemeersch, T. Q. Quek, and H. Wymeersch, "A stochastic geometry model for vehicular communication near intersections," in *Globecom Workshops (GC Wkshps), 2015 IEEE*, pp. 1–6, IEEE, 2015.
- [15] M. Abdulla, E. Steinmetz, and H. Wymeersch, "Vehicle-to-vehicle communications with urban intersection path loss models," in *Globecom Workshops (GC Wkshps), 2016 IEEE*, pp. 1–6, IEEE, 2016.
- [16] J. P. Jeyaraj and M. Haenggi, "Reliability analysis of v2v communications on orthogonal street systems," in *GLOBECOM 2017-2017 IEEE Global Communications Conference*, pp. 1–6, IEEE, 2017.
- [17] T. Kimura and H. Saito, "Theoretical interference analysis of inter-vehicular communication at intersection with power control," *Computer Communications*, 2017.
- [18] B. E. Y. Belmekki, A. Hamza, and B. Escrig, "Cooperative vehicular communications at intersections over nakagami-m fading channels," *Vehicular Communications*, p. doi:10.1016/j.vehcom.2019.100165, 07 2019.
- [19] B. E. Y. Belmekki, A. Hamza, and B. Escrig, "Performance analysis of cooperative communications at road intersections using stochastic geometry tools," *arXiv preprint arXiv:1807.08532*, 2018.
- [20] B. E. Y. Belmekki, A. Hamza, and B. Escrig, "Outage performance of NOMA at road intersections using stochastic geometry," in *2019 IEEE Wireless Communications and Networking Conference (WCNC) (IEEE WCNC 2019)*, pp. 1–6, IEEE, 2019.
- [21] B. E. Y. Belmekki, A. Hamza, and B. Escrig, "On the outage probability of cooperative 5g noma at intersections," in *2019 IEEE 89th Vehicular Technology Conference (VTC2019-Spring)*, pp. 1–6, IEEE, 2019.
- [22] B. E. Y. Belmekki, A. Hamza, and B. Escrig, "Outage analysis of cooperative noma using maximum ratio combining at intersections," in *IEEE 15th Int. Conf. Wireless Mobile Comput. Netw. Commun. (WiMob)*, pp. 1–6, IEEE, 2019.
- [23] T. Bai, R. Vaze, and R. W. Heath, "Analysis of blockage effects on urban cellular networks," *IEEE Transactions on Wireless Communications*, vol. 13, no. 9, pp. 5070–5083, 2014.

- [24] G. Karagiannis, O. Altintas, E. Ekici, G. Heijenk, B. Jarupan, K. Lin, and T. Weil, "Vehicular networking: A survey and tutorial on requirements, architectures, challenges, standards and solutions," *IEEE communications surveys & tutorials*, vol. 13, no. 4, pp. 584–616, 2011.
- [25] S. Subramanian, M. Werner, S. Liu, J. Jose, R. Lupoie, and X. Wu, "Congestion control for vehicular safety: synchronous and asynchronous mac algorithms," in *Proceedings of the ninth ACM international workshop on Vehicular inter-networking, systems, and applications*, pp. 63–72, ACM, 2012.
- [26] T. V. Nguyen, F. Baccelli, K. Zhu, S. Subramanian, and X. Wu, "A performance analysis of csma based broadcast protocol in vanets," in *2013 Proceedings IEEE INFOCOM*, pp. 2805–2813, IEEE, 2013.
- [27] Z. Ding, Z. Yang, P. Fan, and H. V. Poor, "On the performance of non-orthogonal multiple access in 5g systems with randomly deployed users," *IEEE Signal Processing Letters*, vol. 21, no. 12, pp. 1501–1505, 2014.
- [28] Z. Ding, H. Dai, and H. V. Poor, "Relay selection for cooperative noma," *IEEE Wireless Communications Letters*, vol. 5, no. 4, pp. 416–419, 2016.
- [29] Z. Ding, L. Dai, and H. V. Poor, "Mimo-noma design for small packet transmission in the internet of things," *IEEE access*, vol. 4, pp. 1393–1405, 2016.
- [30] S. Singh, M. N. Kulkarni, A. Ghosh, and J. G. Andrews, "Tractable model for rate in self-backhauled millimeter wave cellular networks," *IEEE Journal on Selected Areas in Communications*, vol. 33, no. 10, pp. 2196–2211, 2015.
- [31] N. Deng and M. Haenggi, "The meta distribution of the sinr in mm-wave d2d networks," in *GLOBECOM 2017-2017 IEEE Global Communications Conference*, pp. 1–6, IEEE, 2017.
- [32] M. O. Hasna, M.-S. Alouini, A. Bastami, and E. S. Ebbini, "Performance analysis of cellular mobile systems with successive co-channel interference cancellation," *IEEE Transactions on Wireless Communications*, vol. 2, no. 1, pp. 29–40, 2003.